Composite Structures 165 (2017) 160–170

Contents lists available at ScienceDirect

Composite Structures

journal homepage: www.elsevier.com/locate/compstruct

Modelling of Glulam beams pre-stressed by compressed wood

B. Anshari [a], Z.W. Guan [b,c,*], Q.Y. Wang [c]

[a] Department of Civil Engineering, University of Mataram, NTB, Indonesia
[b] School of Engineering, University of Liverpool, Liverpool L69 3GQ, UK
[c] School of Mechanical Engineering, Chengdu University, Chengdu 610106, China

ARTICLE INFO

Article history:
Received 17 November 2016
Revised 4 January 2017
Accepted 10 January 2017
Available online 16 January 2017

Keywords:
Moisture-dependent swelling
Glulam beam
Compressed wood
Finite element
Pre-stressing
Visco-plasticity

ABSTRACT

Finite element models were, in the first time, developed to simulate the pre-stressing behaviour of Glulam beams with insertion of compressed wood blocks, which were further used to simulate the structural behaviour of the pre-stressed beams subjected to subsequent destructive bending. Here, both the Glulam and compressed wood were modelled as orthotropic elasto-viscoplastic materials. The moisture-dependent, including spring back, swelling of the compressed wood block and the creep of the Glulam were considered in the modelling. The models developed were validated against the corresponding experimental results, with reasonably good correlation in terms of the free swelling, the precamber, initial stress state of the Glulam beams reinforced and load-deflection relationships. With validated models, further studies were then undertaken to investigate effects of the thickness, depth and spacing of compressed wood blocks on the precamber, initial bending stiffness and ultimate load carrying capacity of the beams pre-stressed. The results indicate that there are significant enhancements on the precamber (up to 1/288 of the deflection/span ratio), the initial bending stiffness (up to 23.8%) and the ultimate load carrying capacity (up to 10.4%).

1. Introduction

Reasonable amount of work has been carried out on numerical modelling of mechano-sorptive process in wood and strengthened Glulam beams in the past 3 decades. Research on modelling of moisture movement in wood was undertaken by Koponen et al. [1] to model elastic and shrinkage properties of cell wood structures. Ormarsson et al. [2] developed modelling of the long-term strength and shape stability of timber columns subjected to the moisture variation. Dubois et al. [3] investigated the creep properties of wood under variable climate and moisture changes. Vidal-Sallé and Chassagne [4] developed a constitutive equation for orthotropic nonlinear visco-elastic behaviour using a generalized Maxwell model applied to wood material. Mirianon et al. [5] studied the long-term response of wood under variable load and humidity conditions by using the finite element code Abaqus. The response of wood related to mechanical loading, moisture content changes and time was modelled by using a rheological model of wood, implemented through a user-defined subroutine UMAT. The model was used to simulate the mechano-sorptive properties of wood with good correlation to experimental results obtained from the literature. Dubois et al. [6] simulated the linear viscoelastic, mechano-sorptive behaviour and its effect during change of moisture content on timber.

Martensson [7] developed a model to evaluate behaviour of structural timber under variable humidity conditions. The simulated results show that there is a significant influence of the humidity induced strain on the shrinkage and swelling response. Fortino et al. [8] carried out a 3D finite element analysis on moisture induced stresses for time-dependent problems in timber structures. The constitutive model and the equations to describe the moisture flow across the structure were developed by using a user subroutine in the finite element code Abaqus. The numerical modelling results fit relatively well to the measurements of the stress along both the longitudinal and the radial directions.

Guan et al. [9] developed the finite element models to simulate the structural behaviour of Glulam beams pre-stressed with pultruded GRP tendon. The results showed that the model was capable of simulating the pre-stressing procedure adopted for the Glulam and also indicated a precamber at mid-span of the beam due to transfer of the pre-stressing force. More recently, Kliger et al. [10] presented a study on wood-based beams prestressed with FRP laminates. They demonstrated that applying pre-stressing in FRP materials prior to bonding to tension side of

* Corresponding author at: School of Engineering, University of Liverpool, Liverpool L69 3GQ, UK.
E-mail address: zguan@liverpool.ac.uk (Z.W. Guan).

http://dx.doi.org/10.1016/j.compstruct.2017.01.028
0263-8223/

flexural members is the best way to enhance load bearing capacity through a pre-cambering effect. Kim and Harries [11] made a modelling approach to predict the behaviour of beams strengthened with CFRP composite. The strengthened beams showed improved load-carrying capacity and energy absorption when compared to their unstrengthened counterparts. Valipour and Crews [12] evaluated the efficiency of FE modelling to estimate the load carrying capacity of timber beams flexurally strengthened with externally bonded FRP strips and near surface mounted FRP bars. The model developed demonstrated a good agreement with the test results on the mid-span deflection, and strains at 15 mm from the top and bottom. Modelling of densified wood was undertaken by Guan et al. [13] on structural characteristics of the beam-column connections using compressed wood (CW) dowels and plates. There was reasonably good correlation between the test results and the simulations in terms of moment-rotation relationship. The numerical models also produced information on the contact normal force, the contact shear force and the contact area of various interaction pairs. Anshari et al. [14] developed a preliminary finite element modelling of the upward deflection of Glulam beams reinforced by compressed wood, which was further developed to simulate the initial stress and precamber of Glulam beams pre-stressed [15].

In order to make use of the moisture-dependent and spring back swelling nature of compressed wood, a new approach to strengthen a Glulam beam has been investigated. By inserting the CW blocks with the desired initial moisture content into the top part of a Glulam beam, a precamber and the related initial stresses are built up in the beam, due to the swelling of the CW blocks. However, the way to reinforce the Glulam beam needs to be optimised in terms of the effective size (thickness, depth), location and number of the CW blocks inserted. To undertake such study purely by experimental tests will be time consuming and expensive. The better way forward is to develop numerical models and to apply the validated models to optimise the pre-stressed beams.

This paper presents finite element modelling of Glulam beams pre-stressed by compressed wood. The developed orthotropic elasto-viscoplastic model was employed to simulate the moisture-dependent and spring back swelling of compressed wood blocks after they were inserted in the Glulam beam, which generates a precamber. The subsequent destructive flexural tests of the reinforced beams were also modelled. All numerical outputs were validated against the corresponding experimental measurements. Using the validated model, the influence of the thickness, depth and spacing of CW blocks on the structural response of the reinforced systems was further studied. The output could be used to optimize the structural performance of Glulam beams reinforced by compressed wood, in terms of precamber, initial bending stiffness and load carrying capacity.

2. Experimental work

The pre-stressing technology developed by Anshari et al. [16] is to make use of moisture-dependent swelling and spring back nature of compressed wood. Since there is the largest swelling in the radial direction of compressed wood, the CW block was placed in the way in which its radial direction is coincident with the longitudinal direction of the beam to be strengthened. The CW blocks were conditioned to have moisture content (MC) of 6% prior to the insertion. The beams pre-stressed would be placed in an ambient condition with MC of 12%. After completed insertion of the CW blocks, beams were subjected to measurements of the precamber and strains at selected positions on the beam. The precamber of the beams with insertion of compressed wood blocks was taken manually by using a steel I-beam, long clamp, and also automatically by a transducer placed at mid-span underneath the beam [16]. In addition, the time-dependent free swelling of the conditioned compressed wood blocks was measured [17], which was also used to validate the corresponding FE models. After the precamber is stabilised, i.e. there is no further increasing, four-point bending destructive tests were undertaken on seven structural Glulam beams. The related load-deflection relationships were recorded.

3. Finite element modelling

Both the Glulam and compressed wood were modelled as visco-orthotropic linear elastic materials in tension and as orthotropic elasto-viscoplastic materials in compression in the embedding areas. Firstly, the insertion processes were modelled. Then the moisture-dependent (including spring back) swelling of the compressed wood blocks after they were inserted into the Glulam beams was simulated by implementing a swelling law obtained from experimental measurements. This simulation included the building-up of precamber and the related stress state. Subsequent destructive bending behaviour of the pre-stressed beams was modelled in a quasi-static time-independent domain.

3.1. Constitutive model

The linear orthotropic constitutive equation can be expressed as follows [18]:

$$\{\varepsilon\} = [C^{el}]\{\sigma\} \tag{1}$$

where $\{\varepsilon\}$ is strain tensor, $\{\sigma\}$ is stress tensor and $[C^{el}]$ is orthotropic elastic compliance matrix (6×6), i.e.

$$\{\varepsilon\} = \{\varepsilon_L \varepsilon_R \varepsilon_T \gamma_{LR} \gamma_{LT} \gamma_{RT}\}^T \tag{2}$$

$$\{\sigma\} = \{\sigma_L \sigma_R \sigma_T \tau_{LR} \tau_{LT} \tau_{RT}\}^T \tag{3}$$

$$[C^{EL}] = \begin{bmatrix} 1/E_L & -\upsilon_{RL}/E_R & -\upsilon_{TL}/E_T & 0 & 0 & 0 \\ -\upsilon_{LR}/E_L & 1/E_R & -\upsilon_{TR}/E_T & 0 & 0 & 0 \\ -\upsilon_{LT}/E_L & -\upsilon_{RT}/E_R & 1/E_T & 0 & 0 & 0 \\ 0 & 0 & 0 & 1/G_{LR} & 0 & 0 \\ 0 & 0 & 0 & 0 & 1/G_{LT} & 0 \\ 0 & 0 & 0 & 0 & 0 & 1/G_{RT} \end{bmatrix} \tag{4}$$

where E_L, E_R, E_T are the Young's modulii in the longitudinal (L), radial (R) and tangential (T) directions of wood trunk; G_{LR}, G_{LT}, G_{RT} are the shear modulii in the L-R, L-T, R-T planes; and v_{ij} are the Poisson's ratios ($i, j = L, R, T$).

The above values also have to satisfy the stability requirements below.

$$E_L, E_R, E_T, G_{LR}, G_{LT}, G_{RT} > 0 \tag{5}$$

$$|\upsilon_{LR}| < (E_L/E_R)^{1/2} \tag{6}$$

$$|\upsilon_{LT}| < (E_L/E_T)^{1/2} \tag{7}$$

$$|\upsilon_{RT}| < (E_T/E_R)^{1/2} \tag{8}$$

$$1 - \upsilon_{LR}\upsilon_{RL} - \upsilon_{RT}\upsilon_{TR} - \upsilon_{LT}\upsilon_{TL} - 2\upsilon_{LR}\upsilon_{RT}\upsilon_{TL} > 0 \tag{9}$$

According to the elasto-viscoplastic potential theory, at time t_n the constitutive equation can be express as follows [19].

$$\{\Delta\sigma\}_n = [D](\{\Delta\varepsilon\}_n - \{\dot{\varepsilon}^{vp}\}_n \Delta t_n) \tag{10}$$

or

$$\{\Delta\varepsilon\}_n = [C^{el}]\{\Delta\sigma\}_n + \{\dot{\varepsilon}^{vp}\}_n \Delta t_n \tag{11}$$

where Δt_n is the time stepping length, and $[D]$ and $[C^{el}]$ are the elastic matrix and compliance matrix, respectively. The viscoplastic flow rate is:

$$\{\dot{\varepsilon}^{vp}\}_n = \gamma\langle F\rangle \frac{\partial Q}{\partial\{\sigma\}} = \frac{1}{3}\{\dot{\varepsilon}^{sw}\}_n + \{\dot{\varepsilon}^{cr}\}_n \frac{\partial\bar{\sigma}}{\partial\{\sigma\}} \tag{12}$$

where γ is the fluidity parameter, F and Q are the yield and potential function respectively, $\dot{\varepsilon}^{sw}$ is the effective swelling strain rate, $\dot{\varepsilon}^{cr}$ is the effective creep strain rate, $\bar{\sigma}$ is the effective stress or the deviatoric stress potential.

3.2. Material properties

Material properties of the Glulam and compressed wood used in the modelling were obtained from experimental results of Japanese cedar through shear and compression tests. Orthotropic elastic material properties of the Glulam and compressed wood with 70% compression ratio are listed in Table 1 [17,20].

Strain rate was obtained from measurements of the swelling strain of the compressed Japanese cedar with the initial MC of 6%. The ultimate swelling strain (moisture-dependent swelling and spring back) recorded on the compressed wood in radial and tangential directions with compressive ratio (CR) = 70% was about 17% and 1.5% respectively. Swelling strains in the radial and tangential directions may be expressed by the equations as follows [17].

$$\varepsilon^{R}_{sw} = 0.001694(1 - e^{-0.0772t}) \tag{13}$$

$$\varepsilon^{T}_{sw} = 11.54 \times 10^{-6}(1 - e^{-0.072t}) \tag{14}$$

Compressed wood, with the moisture content set to below the ambient, will swell differently in the radial and tangential directions after absorbing moisture from air and during spring back. Therefore, it is sensible to consider anisotropic swelling in the modelling. In the case of the CW block as a reinforcing material inserted on the top region of the beam, the maximum swelling of the CW block will be obtained when the equilibrium moisture content to the ambient is reached and further spring back is restrained by the surrounding Glulam. Once this condition is satisfied after a certain time, stress relaxation is likely taking place, which is a time-dependent decrease of stress under the condition of a constant deformation.

On the other hand, on the Glulam which restrains the expansion of CW block when there is no more deformation (excluding fluctuations) under a specific pressure (stress), then creep is likely to occur. Therefore, the user-defined creep law was implemented into ABAQUS to simulate the non-linear swelling/expansion of compressed wood and creep of the Glulam.

In this study, the creep law was derived from swelling strain in Eq. (13) as stated below in Eq. (15). This law was applied to describe the creep behaviour of compressed wood [15]

$$\dot{\varepsilon}^{c}_{CW} = \left(e^{-0.065\sigma}\right) \times \left(A(1 - e^{-B(t+\Delta t)}) - A(1 - e^{-Bt})\right) \tag{15}$$

where $A = 0.1694$; $B = 8.936 \times 10^{-7}$; $t = time$ (in second), and for creep law which was applicable for the Glulam part can be formulated as follows:

$$\dot{\varepsilon}^{c}_{Gl} = \left(e^{-0.1\sigma}\right) \times \left(0.0159(1 - e^{-B(t+\Delta t)}) - 0.0159(1 - e^{-Bt})\right) \tag{16}$$

Regarding the anisotropic swelling behaviour of compressed wood, the swelling rate in each material orientation can be expressed as

$$\dot{\varepsilon}^{sw}_{ii} = r_{ii}\frac{1}{3}\dot{\varepsilon}^{sw}, \quad i = L, R, T \tag{17}$$

where $\dot{\varepsilon}^{sw}_{ii}$ is swelling strain rate (s^{-1}) in i direction, $\dot{\varepsilon}^{sw}$ is volumetric swelling strain rate (s^{-1}) and r_{ii} are the ratios of swelling in i direction. In this study, they were calculated as $r_{LL} = 0$; $r_{RR} = 1.67$; $r_{TT} = 0.15$.

3.3. Finite element simulation

In the modelling of the Glulam beams, user-defined subroutines of creep law and swelling law were implemented into the Abaqus main programme. The swelling of compressed wood was modelled by implementing the measured swelling strain rate into the swelling model in Abaqus. Subroutines of the swelling law and creep law were developed in Fortran codes, which were used to describe time-dependent deformations of CW blocks and Glulam beams respectively.

Fig. 1 shows the interaction between a CW block and a Glulam beam. Similar to the test, there was a gap set on each side of the block in the tangential direction to allow moisture flow through these gaps to make moisture-dependant swelling of the compressed wood block more efficiently in the experiment. In addition, 1 mm gap was also made between the bottom of a CW block and a hole on the Glulam for the same purpose. The surface to surface contact was employed to model the interaction between the CW and the Glulam, with the former and the latter being defined as the master surface and slave surface respectively. As the delamination was not observed during the test, the laminates in the Glulam beam were tied.

3.3.1. Modelling the pre-stressing of Glulam beams

3-D finite element models were developed to simulate the precamber and the pre-stressing state of the Glulam beams reinforced. The model of the Glulam beam is 3800 mm in length, 200 mm in depth, 120 mm in width and 3600 mm in span length complied with requirements for a structural member specified in BS EN 408:2003, as shown in Fig. 2. Dimensions of the compressed wood block were $65 \times 65 \times 45$ mm^3 coinciding with the L, T, and R directions, respectively. This horizontally laminated beam consists of

Table 1
Material properties used in the FE models.

Material	Modulus of elasticity (MPa)					
Japanese cedar	E_L	E_R	E_T	G_{LR}	G_{Lt}	G_{RT}
	8017	753	275	972	784	31
Compressed wood*	32858	3111	5061	878	5717	1590
	Poisson's ratio					
	υ_{LR}	υ_{LT}	υ_{RL}	υ_{TL}	υ_{RT}	υ_{LTR}
Japanese cedar	0.54	0.48	NA	0.05	0.58	0.42
Compressed wood*	0.33	0.41	0.40	0.30	0.03	0.06

* Compression ratio: 70%.

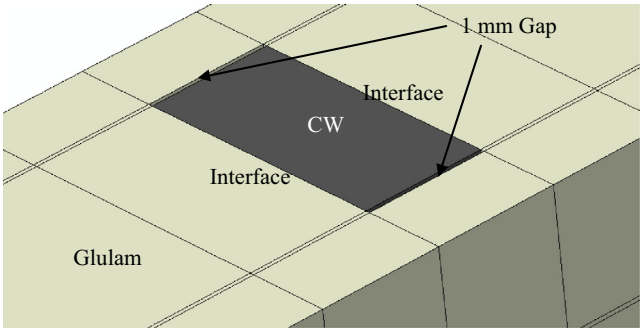

Fig. 1. The gap between CW block and Glulam.

eight laminates with the thickness of 25 mm each. There were two beams not only reinforced by compressed wood blocks, but also by a compressed wood lamina with a thickness of 25 mm at the bottom extreme layer to investigate the influence of the bottom CW lamina attached, as shown in Fig. 2. Similar to the experimental setting up, the CW block was placed in a way in which its radial direction was coincident with the longitudinal direction of the beam to be strengthened.

The mesh density in the region around the compressed wood block was much higher than other regions, which was determined by mesh sensitivity studies with the balanced accuracy and CPU time. Also the mesh on the CW lamina was slightly finer than that of the adjacent upper Glulam lamina. This beam was reinforced by five CW blocks and a CW lamina was meshed by 82,568 solid elements with reduced integration and hourglass control (C3D8R).

3.3.2. Modelling destructive tests of the pre-stressed Glulam beams

The final stage of the FE analysis was to simulate the destructive flexural tests of Glulam beams, following modelling of the pre-stressing process until there was hardly any increase on precamber. The beam was assumed to be simply supported at a span of 3600 mm, similar to that in the test. In the model, the mean failure deflection obtained from tests was applied to simulate the structural behaviour of Glulam beams. There were four types of beams reinforced with 3, 5 and 7 CW blocks (45 mm thick), respectively, either with or without CW lamina attached to the bottom extreme fibre, and also there were three control beams without reinforcement.

4. Results and discussion

4.1. Free and constrained swelling

4.1.1. Free expansion in R and T directions

Fig. 3 shows the predicted final free expansion in the radial direction after 60 days, which indicates a 7.2 mm expansion displacement in comparison to the initial dimension of 45 mm in the radial direction, i.e. a swelling strain of 16%. The progressive swelling strains in the R direction obtained from the FE model are compared with the corresponding test results, which gives reasonably good correlation. The slightly lower predictions of the swelling strains may be due to the small constraint offered by low stiffness (1 N/m) springs that connected the compressed wood block and the fixed base plate in the model, which were used to avoid numerical singularity. The final swelling state of the CW block is also displayed (Fig. 3a).

Similarly, the free expansion of a CW block in the tangential direction after 60 days reached 0.37 mm (0.175 + 0.193), from the initial thickness of 25 mm in the T direction, as shown in Fig. 4a. The growth of the swelling strains in the T direction during 60-day test period is shown in Fig. 4b. It is evident that the predicted swelling deformations are in a good agreement with the measurements.

4.1.2. Constrained swelling

In order to investigate how an overlap dimension between a CW block and a hole in the Glulam beam along its longitudinal direction affect the local strain due to the swelling of the CW block, insertion processes were simulated by using 30 mm thick CW blocks with various oversized dimensions in their R direction. A contour plot of the simulated strains around a CW block is shown in Fig. 5. Clearly, due the overlap large localised initial tensile and compressive strains (so stresses) were generated in areas on the Glulam adjacent to both the gaps and in the interface between the CW block and the Glulam, respectively. Also, with increasing the oversize, the strains generated were increased. There are clearly separated areas corresponding to the tensile and compressive strains, with the size varied in relation to the overlap. Table 2

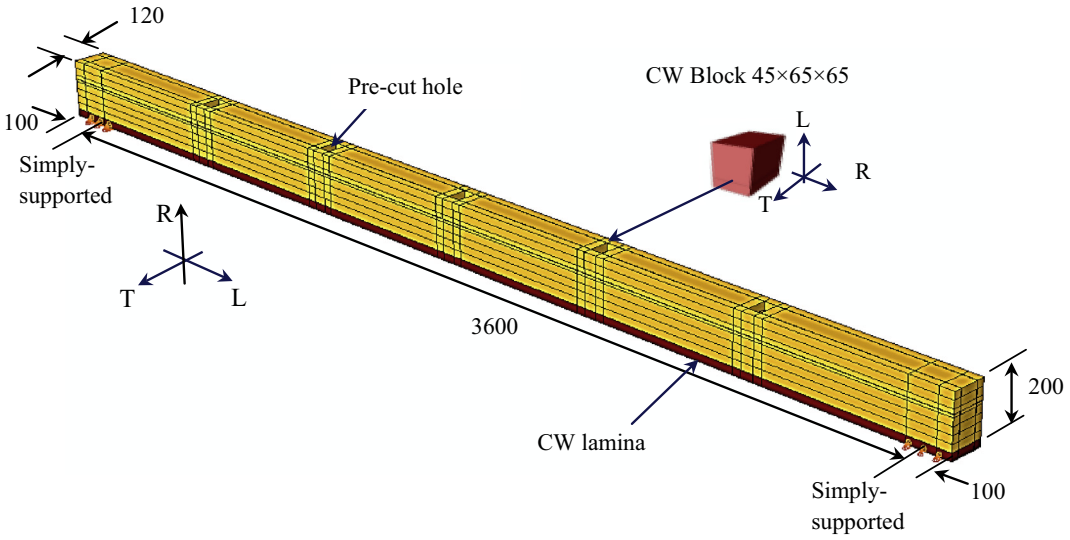

Fig. 2. The beam reinforced by five 45 mm thick CW blocks with a CW lamina on the bottom (all dimensions: mm).

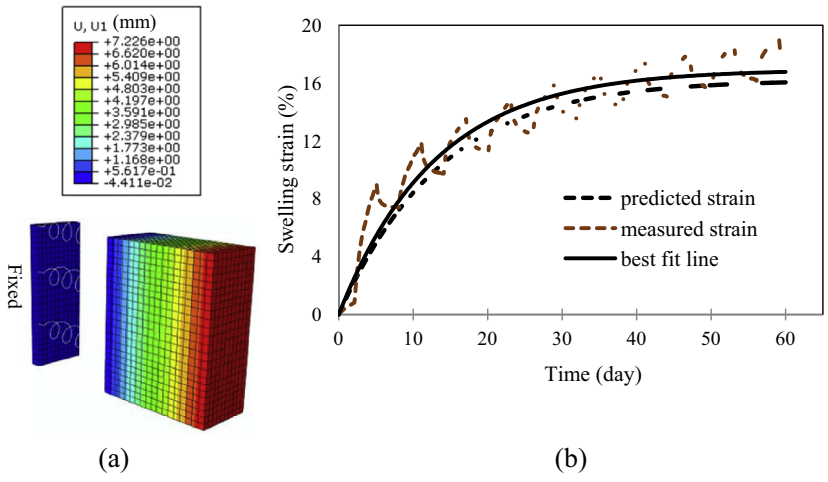

Fig. 3. (a) Free expansion in the radial direction (U_1) of the CW block; (b) Comparison of the measured and the simulated swelling strains of the CW in the radial direction.

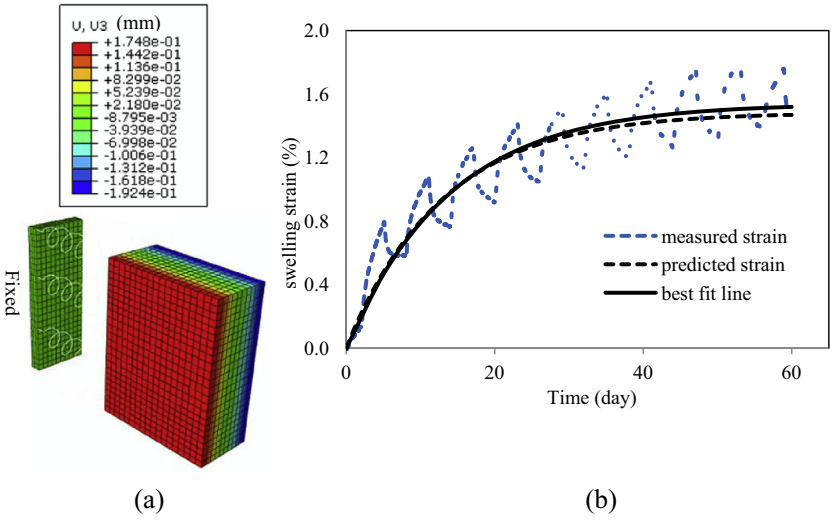

Fig. 4. (a) Free expansion in the tangential direction (U_3) of the CW block; (b) Comparison of the measured and the predicted swelling strains of the CW block in the tangential direction.

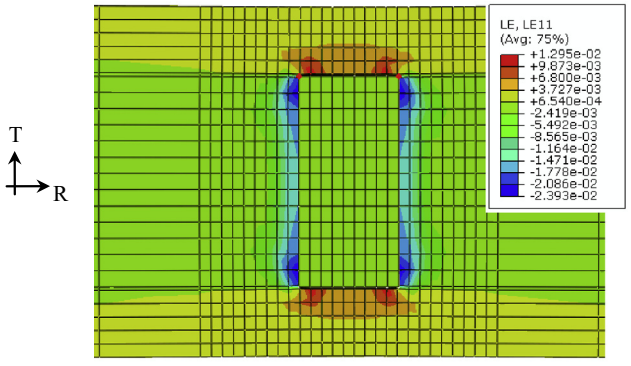

Fig. 5. Distribution of the longitudinal strains (mm/mm) after the insertion of a CW block with an overlap of 0.5 mm at both left and right sides of the block.

summarizes the predicted strains which were generated by insertion of CW blocks with an oversize of 0.25, 0.5, 0.75 and 1 mm, respectively. In general, the generated strains increase with increasing oversize of the CW block as expected. The maximum strain on the top extreme fibre at mid-span is 3300 micro-strain corresponding to the oversize of 1 mm, which is quite significant.

Table 2
Summary of the generated strains with different oversized CW blocks.

No	Total oversize (mm)	Strain (microstrain)
1	0.25	850
2	0.5	1700
3	0.75	2500
4	1	3300

4.2. Pre-stressing of Glulam beams

Fig. 6 shows the simulated upward deflection, i.e. precamber, for a beam reinforced by seven CW blocks with a thickness of 45 mm and one CW lamina. The precamber at mid-span was 8.4 mm (equal to 1/429 of deflection/span ratio) due to the swelling of CW blocks after they were inserted into the top region of the beam for 60 days.

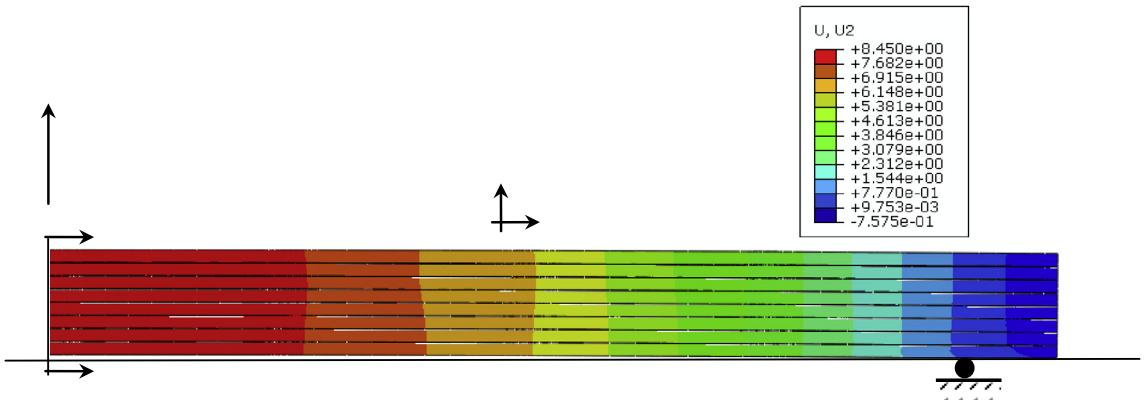

Fig. 6. Modelling of precamber for a beam reinforced by seven 45 mm thick CW blocks and one CW lamina.

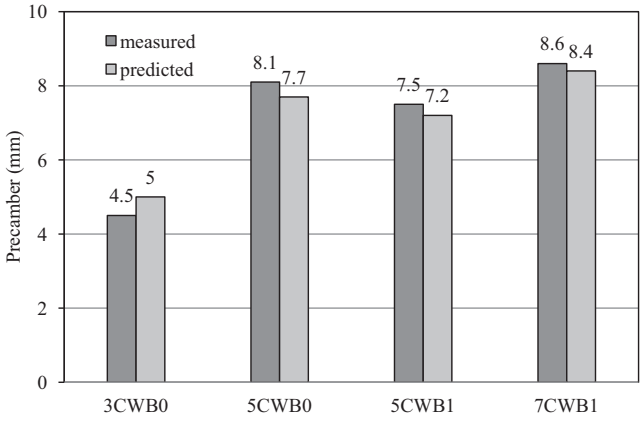

Fig. 7. Comparisons of the predicted and measured precamber deflections of beams reinforced by three (no CW lamina), five (with and without CW lamina) and seven (one CW lamina) 45 mm thick CW blocks.

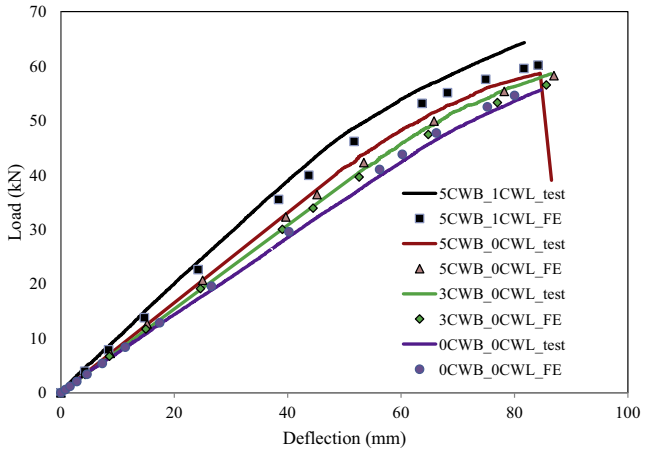

Fig. 8. Load-deflection curves from the destructive bending tests and the corresponding FE simulations of the glulam beams.

Fig. 7 shows the comparisons of the predicted and the experimental precamber for three beams pre-stressed with different numbers of CW blocks. Reasonably good correlation was obtained. In general, the predicted precamber was slightly lower than those obtained from the tests, except for the beam reinforced by three CW blocks without lamina. The FE simulations shown in Fig. 7 also indicate that the beam reinforced with the same amount of CW blocks, but also by a CW lamina, produced the lower precamber than the beam without CW lamina. Similar results were obtained in the experimental results. Thus, although an extra CW lamina on the bottom extreme fibre might avoid premature failure of splitting there in the destructive bending test, it also cancelled out some precamber. By increasing the number of CW blocks from five to seven, the predicted precamber increased by 16.7%, which is correlated to the measurements. With the extra CW lamina reinforcement at the extreme bottom fibre but the same amount of CW blocks, the precamber would decrease by 6.5%. The highest precamber predicted was 8.4 mm for the beam reinforced by seven 45 mm thick CW blocks and one layer CW lamina, which was slightly lower than the measured one of 8.6 mm.

4.3. Modelling results of destructive tests of the Glulam beams

Fig. 8 shows the comparisons of load-deflection relationships from the FE simulations and the experimental measurements. In general, the predicted flexural stiffnesses were slightly lower than those of the experimental ones, except for the unreinforced beam. In terms of the maximum load, the differences between the simulations and the measurements were 7.7%, 0.8%, and 3% for beams reinforced by five 45 mm thick CW blocks and a CW lamina, by five 45 mm thick CW blocks without CW lamina, as well as by three 45 mm thick CW blocks without CW lamina, respectively. All modelling results show the similar trend, with the curves demonstrating overall linear features until a certain load level, which was varied from beam to beam from 40 and 45 kN.

5. Study on the influence of compressed wood block configurations

Using validated models, studies were undertaken to investigate the effects of the thickness, depth and spacing of compressed wood blocks on the precamber, initial bending stiffness and ultimate load carrying capacity of the beams pre-stressed. Table 3 shows the variables considered in the study, which also indicates the ratio of the total volume of CW as a reinforcing material to the total volume of the Glulam beam, varying between 0.8% and 2.7%.

In the computer models, there were two steps corresponding to simulations of the swelling deformations of the CW blocks and the subsequent bending tests of the Glulam beams strengthened. The 'VISCO' analysis and the 'GENERAL ANALYSIS' were used to simulate the precamber of the beam with embedded CW blocks and the subsequent quasi-static bending behaviour of the pre-stressed Glulam beams.

Table 3
Summary of various CW geometric parameters studied.

No.	Space(a) mm	Thickness (t) mm			Width (b) mm	Depth (d) mm	Number of CW blocks	Fraction volume of CW (%)		
1	600	30	40	50	75	65	5	0.80	1.07	1.34
2	600	30	40	50	75	80	5	0.99	1.32	1.64
3	600	30	40	50	75	95	5	1.17	1.56	1.95
4	450	30	40	50	75	65	7	1.12	1.50	1.87
5	450	30	40	50	75	80	7	1.38	1.84	2.30
6	450	30	40	50	75	95	7	1.64	2.19	2.73

5.1. CW block thickness, depth and spacing against the precamber

There were three thicknesses of the CW block studied in the beam model, i.e. 30, 40 and 50 mm. According to experimental measurements and numerical modelling results, the thickness exceeding 50 mm is likely to cause local splitting damage on the top lateral edges of Glulam outside the CW block due to a large local expansion of the block. For the various thicknesses of CW blocks studied, their width was kept at 75 mm. Similar to the test set up, the 1 mm gap was kept on the lateral edges of the each block in the numerical model.

There were also three depths of the CW block considered in the parametric studies, while keep its thickness as 40 mm. Here, a 1 mm gap was again set up between the bottom of the CW block and the Glulam, as did with the test set up. The depths of the CW blocks investigated are 65, 80 and 95 mm. The reason for selecting the maximum depth as 95 mm is that this depth is approaching half of the beam depth (200 mm). A depth exceeding it is likely to cancel out some of the precamber generated in the Glulam beam due to the swelling of CW blocks located in the lower half of the beam depth.

The space between two CW blocks along the beam span was set as 450 mm and 600 mm respectively, corresponding to 5 and 7 CW blocks. The reason to choose seven blocks as the upper bound of the reinforcement is that the effective space between CW blocks is about 450 mm for the largest CW block, i.e. $75 \times 50 \times 95$ (in mm). Based on the trial FE modelling, a space below 450 mm will likely lead an excessive expansion of the CW block and cause local damage on the Glulam.

From the parametric studies of the swelling of the inserted CW blocks, the precamber values at midspan of all beams modelled were obtained. The maximum value of the precamber shown in Fig. 9 is 12.5 mm, when the beam was reinforced by seven CW blocks with thickness of 40 mm and depth of 95 mm. Fig. 9 illustrates a precamber corresponding to the CW volume fraction to the Glulam volume. Clearly, the highest precamber was obtained when the largest CW volume is embedded in the Glulam beam. However, the increase of the CW volume fraction does not follow a linear relationship, so does the increase of the precamber, although both show a general upward trend. From Fig. 9, it can be noted that the effective reinforcement may be realised when the precamber bar is above the line of the CW volume fraction. As an example, effective reinforcements seem to be the beam reinforced by five CW blocks with thicknesses of 30 mm and 40 mm in a depth of 65 mm. On the other hand, the less effective reinforcement occurs when pre-camber below the line of the CW volume fraction, i.e. 5CWB_T50_D95 and 7CWB_T50_D95, where T and D represent the thickness and depth of CW block respectively. However, the CW volume fraction is relatively small. Even the highest fraction is just 2.7%, which corresponds to a pre-camber/span ratio of 1/288.

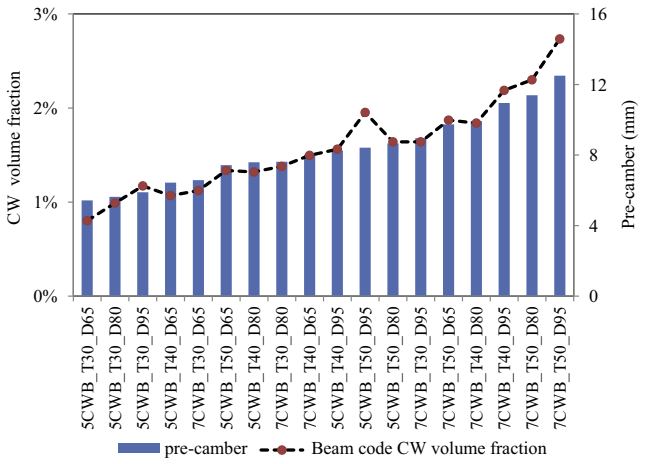

Fig. 9. The precamber against the CW volume fraction of all beams studied.

Figs. 10a and 10b show the bending stress distributions of the beams reinforced by CW blocks with different thickness, space and depth. It can be seen that the thicker the CW block, the higher the stress generated at a larger area of the Glulam beam along the edge of the CW at the top extreme fibre. Fig. 10b, corresponding to the CW thickness of 50 mm, indicates 11.6% higher bending stresses than those of the beam reinforced with the CW block thickness of 30 mm (Figs. 10 (a)), i.e. 36.2 MPa. Although the maximum bending stress values are high, they only appear at small regions on the top extreme fibre. This is unlikely to cause local damage there, which was evidenced in the experimental work.

Fig. 11 displays bending strain distributions of the beam reinforced by seven CW blocks with a thickness of 30 mm for a given depth of 65 mm. It can be seen that there are spots of high strain at the top extreme fibre around the four corners of the CW block. With increasing CW block thickness and depth, the tensile bending strains generated are increased, as expected. The study also shows that by increasing the CW thickness from 30 mm to 40 mm and 50 mm but with the related depth of 95 mm and 80 mm, the corresponding tensile strains (0.01203 and 0.01309) are increased by 28 and 39% respectively, at the top extreme fibre. This indicates that the increase of the CW block depth to the half-way through the beam depth is not effective. Similarly, at the bottom extreme fibre, the compressive bending strains are increased by 12 and 16%, when the CW thickness is increased in the same way as the above.

There were 19 beams modelled in the parametric studies, including one beam without CW reinforcement for control purposes. In the model validation, the beam same as the one shown in Fig. 11 was simply supported with a downward deflection of 80 mm applied at mid-span. Its maximum bending stresses at the top and bottom extreme fibres are 34.6 and 36.4 MPa, respectively. The lower stress on the top extreme fibre is due to the resistance to the further compression contributed by the CW blocks.

Relationships between the CW block thickness and the precamber of the beam strengthened are shown in Fig. 12, for a given CW block depth of 65 mm. It can be seen that the larger CW block thickness produces the higher precamber, so does the smaller spacing between CW blocks. Clearly, for a given CW block depth,

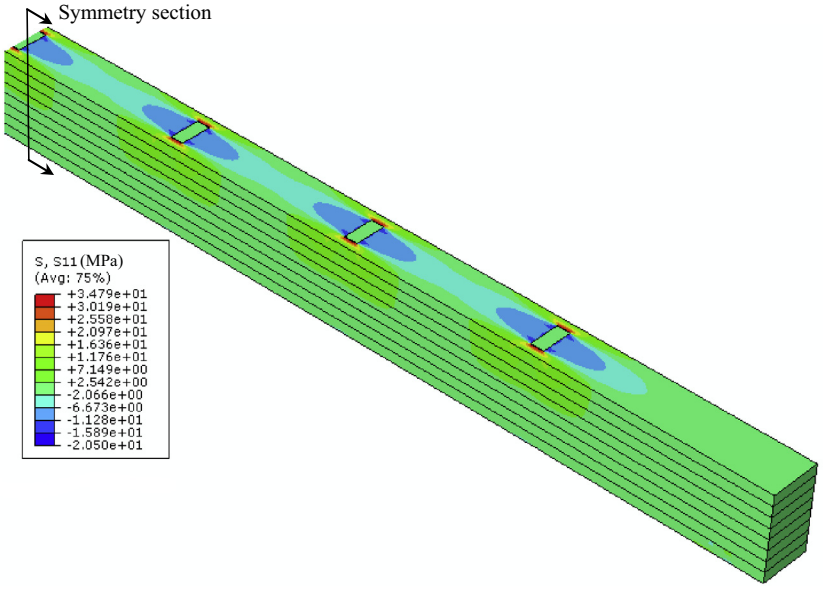

(a) Seven CW blocks with a thickness of 30 mm and a depth of 65 mm,

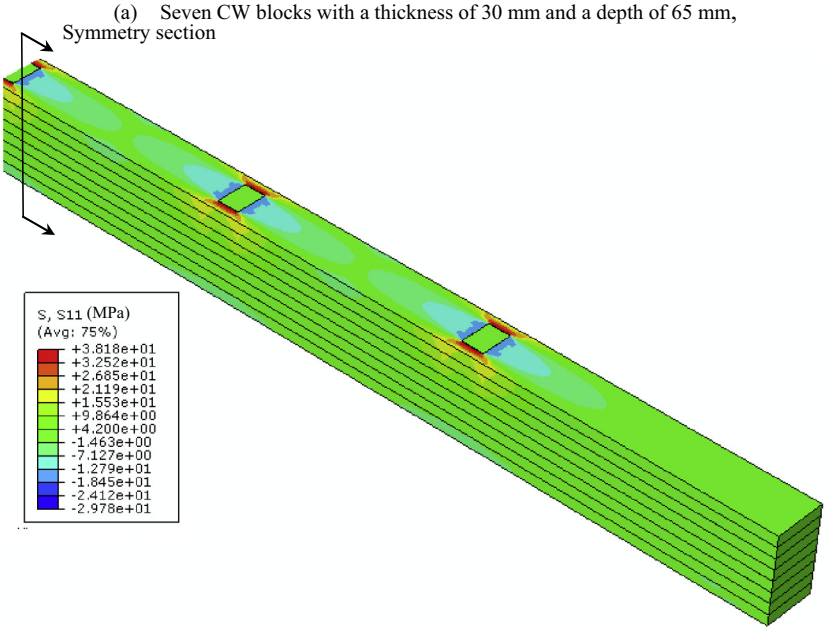

(b) Five CW blocks with a thickness of 50 mm and a depth of 80 mm.

Fig. 10. Bending stress distributions for beams reinforced with CW blocks in different thicknesses and depths.

the improvement of precamber follows a linear relationship with the increasing of CW block thickness. With increasing the thickness by 66.7%, the precamber is increased by 36.8% and 48.0% corresponding to a CW block spacing of 600 mm and 450 mm respectively. The smaller spacing means a larger CW volume fraction, which contributes a higher precamber in the strengthened Glulam beam.

Fig. 13 illustrates relationships between the precamber and the CW block thickness with CW block spacing, for a given CW block depth of 80 mm. The precamber is increased with the increase of CW block thickness, as expected. By decreasing the CW block spacing from 600 mm to 450 mm, the precamber of the beams reinforced by 30, 40 and 50 mm thick of CW blocks is increased by 34.9, 30.7 and 31.5%, respectively. These results indicate that the smaller block spacing and the deeper block (up to 2/5 of the beam depth) are more effective to enhance the precamber than increasing the block thickness.

Relationships between the CW block thickness and the precamber generated for a given CW block depth of 95 mm are presented in Fig. 14. By increasing the CW block depth up to 46% (i.e. from 65 mm to 95 mm), it enhances the precamber by 36.0, 36.5 and 28.3% for the beams reinforced by 30, 40 and 50 mm thick CW blocks respectively, for a CW block spacing of 450 mm (Figs. 8 and 10). Similarly, with the same increase on the CW block depth but for a spacing of 600 mm, improvements on the precamber are 8.5, 28.3 and 13.3%. For both the CW block spacing, the enhancement on the precamber is not significant by increasing the CW block depth from 80 mm to 95 mm (Figs. 13 and 14). This means that the block depth of 80 mm is likely close to the optimum one.

5.2. CW block thickness, depth and spacing against the ultimate load

Fig. 15 shows relationships between the ultimate load and the CW block thickness, and the CW block spacing, in relation to the

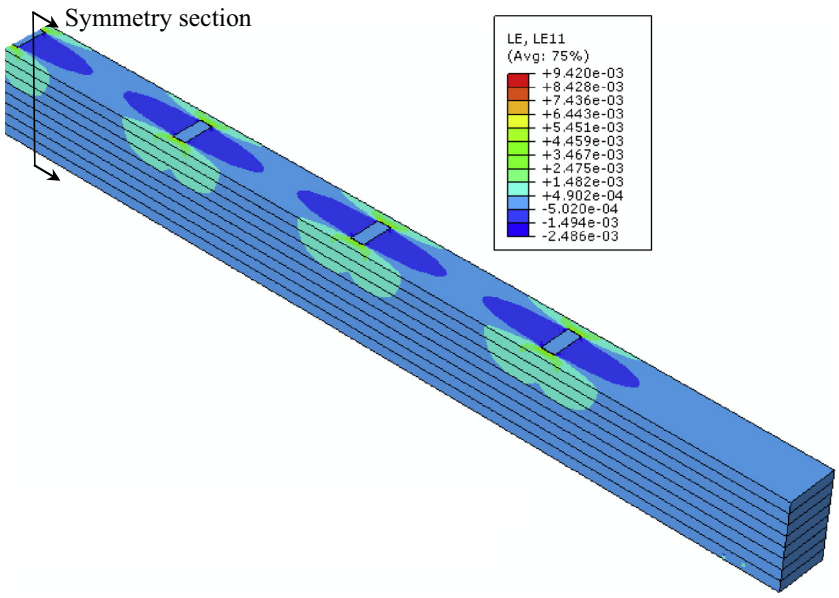

Fig. 11. Bending strain distribution due to the CW swelling for the beam reinforced seven CW block with thickness and depth of 30 mm and 65 mm.

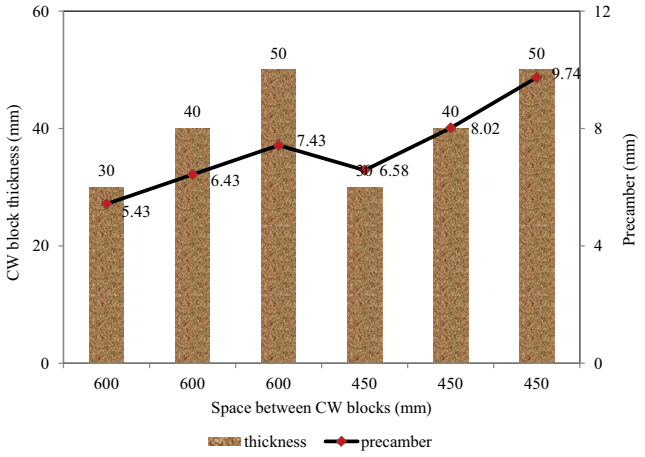

Fig. 12. Variation of CW block thickness against the precamber of the reinforced beam for a given CW block depth of 65 mm.

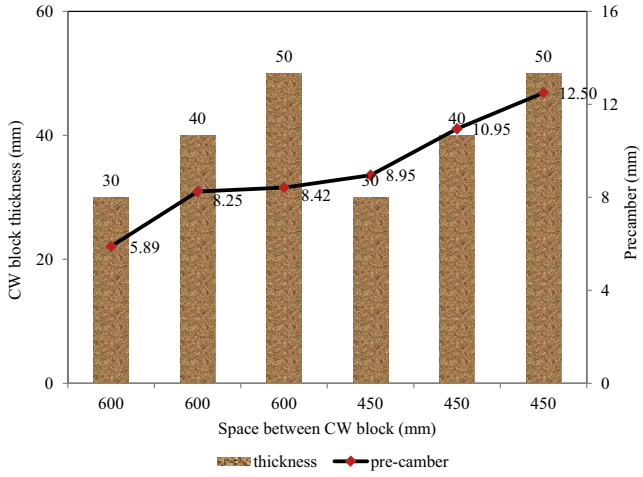

Fig. 14. Variation of the CW block thickness against the precamber of the beams reinforced for a given CW depth of 95 mm.

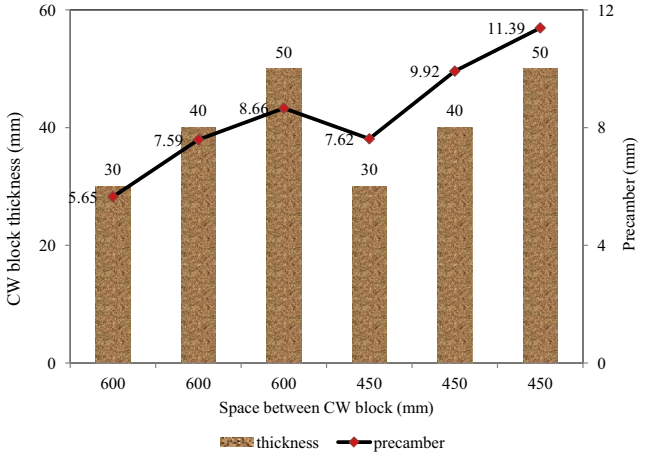

Fig. 13. Variation of CW block thickness against the precamber of the beams reinforced for a given CW block depth of 80 mm.

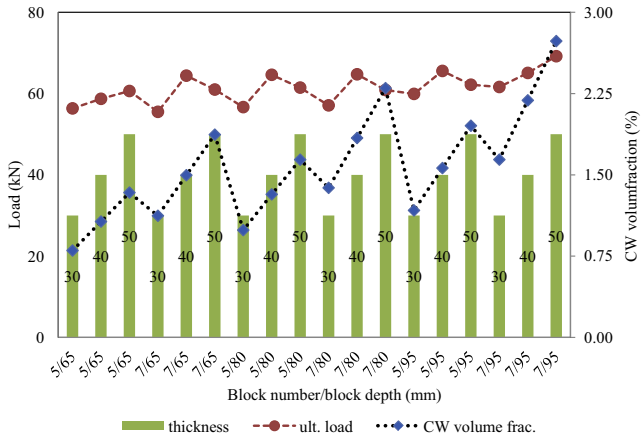

Fig. 15. Variation of the CW volume fraction against the ultimate load of Glulam beams reinforced by CW blocks with different configurations.

CW volume fraction with different depths of the CW block. It can be seen that the increase on CW block thickness leads to an enhanced ultimate load in general, especially true to the cases in relation to the 5-block reinforcement with the smallest block depth and the 7-block reinforcement with the largest block depth. The smallest block thickness is certainly corresponding to the lowest ultimate load for all reinforcing groups. However, this is not always true for the largest block thickness investigated. In fact, the average ultimate load for the beams reinforced by 40 mm thick CW blocks but with different depths reaches 63.9 kN, which is 10.4% and 8.1% higher than those averages of the beams reinforced by 30 mm and 50 mm thick blocks with different depths respectively, i.e. 57.9 and 62.6 kN. However, if referred to CW block depth, the average ultimate loads are 59.4, 60.9 and 63.9 kN for beams reinforced by CW blocks with depths of 65, 80 and 95 mm respectively. The average ultimate load for the beams reinforced by seven CW blocks is slightly higher than that of the beams by five CW blocks, i.e. 62.2 kN in comparison to 60.7 kN. In terms of the improvement contributed by CW volume fraction, with increasing this fraction by 1.07, 1.31 and 1.56%, the corresponding ultimate loads are enhanced by 8.2, 7.4 and 9.3% respectively, with respect to CW block depths of 65, 80 and 95 mm.

As a consequence of precamber, the initial bending stiffness would be increased. There are three groups of the parametric study models with different CW reinforcing arrangements and one control beam without any reinforcement. Fig. 16 shows the load-deflection relationships of all beams reinforced by CW blocks with the same thickness of 30 mm. In general, all curves show a similar trend, with an initial linear feature until a certain load level, followed by mild non-linear behaviour. All beams reinforced by CW blocks indicate a significant enhancement on the initial bending stiffness, which is varied from 12.1% (771 N/mm) to 32.7% (913 N/mm) in comparison to that of the control beam model, i.e. 688 N/mm. The average initial bending stiffness of this beam group reinforced is 793 N/mm, which is 15.3% higher than the control beam.

Fig. 17 illustrates the enhancement on the initial bending stiffness of the beams reinforced by five or seven CW blocks with the same thickness of 40 mm but various depths. From the load-deflection relationships all curves exhibit linear behaviour until the transition point of changing slope, followed by a slight softening until the end. The average initial bending stiffness is 828 N/mm or 20.4% higher than that of the control beam, which is also 4.4% higher than that of the beams reinforced by 30 mm thick CW blocks (Fig 16), i.e. 793 N/mm.

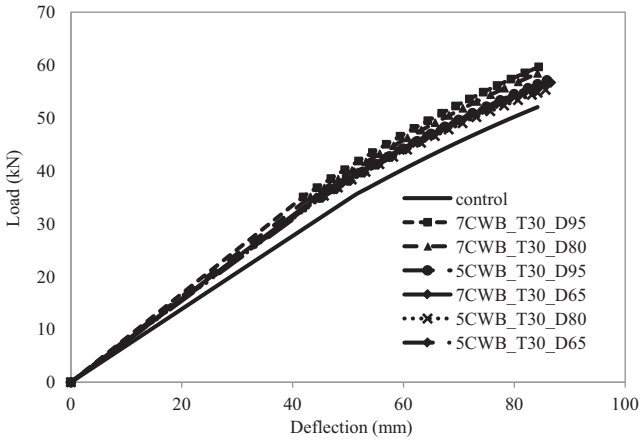

Fig. 16. Load-deflection curves of beams reinforced by CW blocks with thickness of 30 mm, but different depth and spacing.

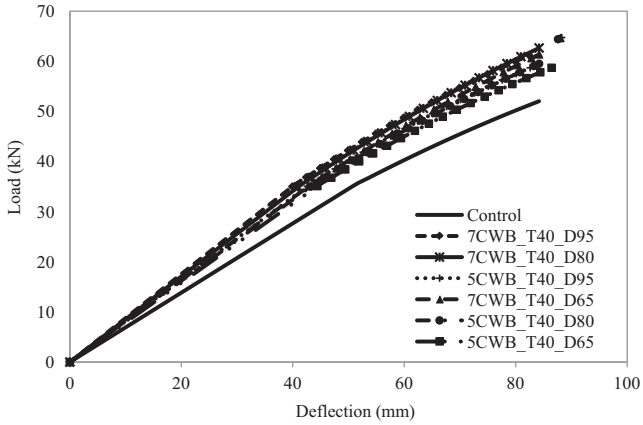

Fig. 17. Load-deflection curves of beams reinforced by CW blocks with thickness of 40 mm, but different depth and spacing.

In the case of the beams reinforced by CW blocks with the same thickness of 50 mm but different depth and spacing, the average initial bending stiffness of these six beams modelled is 852 N/mm or 23.8% higher than that of the control beam.

6. Conclusions

3D finite element models were, for the first time, developed to simulate precamber of Glulam beams pre-stressed using compressed wood (CW) blocks with various configurations. The precondition with a lower moisture content than the ambient one was set as an initial condition in the CW blocks. Here, the moisture dependent and spring back swelling of the CW block restrained by the surrounding Glulam was then modelled using elasto-viscoplasticity, with time-dependent swelling laws describing the swelling in the three principal directions, i.e. radial, tangential and longitudinal. The user-defined creep laws were also implemented into ABAQUS to simulate the non-linear swelling of the compressed wood and creep of the Glulam. Furthermore, destructive tests of the pre-stressed Glulam beams with different reinforcing arrangements were simulated. The predicted initial strain states (therefore stress states), the precamber and the subsequent destructive bending behaviour of the pre-stressed Glulam beams were validated against the corresponding experimental results with reasonably good correlation. This includes the beams reinforced by three (no CW lamina), five and seven (one CW lamina) 45 mm thick CW blocks. The highest precamber predicted was 8.4 mm for the beam reinforced by seven 45 mm thick CW blocks and one CW lamina, which was slightly lower than the measured one of 8.6 mm.

Using validated models, further studies were undertaken to investigate the effects of the thickness, depth and spacing of compressed wood blocks on precamber, initial bending stiffness and ultimate load carrying capacity of the beams pre-stressed. It was found that the enhancement on the initial bending stiffness of the pre-stressed beams is significant with an average of 20%. However, such enhancement on the ultimate bending capacity is limited (10%). Moreover, for the thicknesses of the CW block investigated with an insertion depth of 40% of the beam depth, the precamber was increased by >30% when reduce the CW spacing by 25%. It was also found that even with the CW fraction being just 2.7%, the corresponding enhancement on precamber/span ratio can reach 1/288 for the beam studied.

It is worth pointing out that the current study is based on the short-term experimental data and numerical modelling, which shows quite promising results for this simple and novel

prestressing technique. Although the 70% compression ratio on compressed wood will likely offer sustainable spring back to maintain the prestressing status of the strengthened beam irrespective seasonal temperature and moisture changes, it may be necessary to monitor the structural performance through its service time, at least in the first 10 years, to ensure the validity of the technique.

Acknowledgements

Authors are grateful to the Higher Education Directorate General, Ministry of National Education, Republic of Indonesia for the financial support of this Project.

References

[1] Koponen S, Toratti T, Kanerva P. Modelling elastic and shrinkage properties of wood based on cell structure. Wood Sci Technol 1991;25(1):25–32.
[2] Ormarsson S, Dahlblom O, Petersson H. A numerical study of the shape stability of sawn timber subjected to moisture variation. Wood Sci Technol 2000;34(3):207–19.
[3] Dubois F, Randriambololona H, Petit C. Creep in wood under variable climate conditions: numerical modeling and experimental validation. Mech Time-Depend Mater 2005;9(2):173–202.
[4] Vidal-Sallé E, Chassagne P. Constitutive equations for orthotropic nonlinear viscoelastic behaviour using a generalized Maxwell model Application to wood material. Mechan Time-Depend Mater 2007;11(2):127–42.
[5] Mirianon F, Fortino S, Toratti T. A method to model wood by using ABAQUS finite element software. Helsinki: VTT Technical Research Centre of Finland; 2008.
[6] Dubois F, Husson JM, Sauvat N, Manfoumbi N. Modeling of the viscoelastic mechano-sorptive behavior in wood. Mechan Time-Depend Mater 2012;16(4):439–60.
[7] Martensson A. Creep behavior of structural timber under varying humidity conditions. J Struct Eng 1994;120(9):2565–82.
[8] Fortino S, Mirianon F, Toratti T. A 3D moisture-stress FEM analysis for time dependent problems in timber structures. Mech Time-Depend Mater 2009;13(4):333–56.
[9] Guan ZW, Rodd PD, Pope DJ. Study of Glulam beams pre-stressed with pultruded GRP. Comput Struct 2005;83(28–30):2476–87.
[10] Kliger R, Haghani R, Brunner M, Harte AM, Chober KU. Wood-based beams strengthened with FRP laminates: improved performance with pre-stressed systems. Euro J Wood Wood Prod 2016;74(3):319–30.
[11] Kim YJ, Harries KA. Modeling of timber beams strengthened with various CFRP composites. Eng Struct 2010;32(10):3225–34.
[12] Valipour HR, Crews K. Efficient finite element modelling of timber beams strengthened with bonded fibre reinforced polymers. Constr Build Mater 2011;25(8):3291–300.
[13] Guan ZW, Komatsu K, Jung K,Kitamori A. Structural characteristics of beam-column connections using compressed wood dowels and plates. In: Proceedings of the 11th world conference on timber engineering (WCTE), 20–24 June 2010. Riva del Garda, Trentino, Italy.
[14] Anshari B, Guan ZW, Komatsu K. Finite element modeling of the pre-camber of Glulam beams reinforced by compressed wood the 11th World Conference on Timber Engineering (WCTE) 20–24 June 2010, Riva del Garda, Trentino, Italy; 2010.
[15] Anshari B, Guan ZW. Numerical modelling of the initial stress and upward deflection of glulam beams pre-stressed by compressed wood. Appl Mech Mater 2014;493:408–13.
[16] Anshari B, Guan ZW, Kitamori A, Jung K, Komatsu K. Structural behaviour of glued laminated timber beams pre-stressed by compressed wood. Constr Build Mater 2012;29:24–32.
[17] Anshari B, Guan ZW, Kitamori A, Jung K, Hassel I, Komatsu K. Mechanical and moisture-dependent swelling properties of compressed Japanese cedar. Constr Build Mater 2011;25(4):1718–25.
[18] ABAQUS Standard: User's Manual, Hibbitt, Karlsson & Sorensen, Inc.; 2012.
[19] Owen DRJ, Liu GQ. Elasto-viscoplastic analysis of anisotropic laminated plates and shells. Eng Comput Int J Comput-Aided Eng 1985;2(2):90–5.
[20] Anshari B. Structural behaviour of glued laminated timber beams reinforced by compressed wood [Ph.D. thesis]. University of Liverpool; 2012.